Inorganic Chemistry

Article

pubs.acs.org/IC

Di- and Trinuclear Mixed-Valence Copper Amidinate Complexes from Reduction of Iodine

Andrew C. Lane,[†] Charles L. Barnes,[†] William E. Antholine,*[,‡] Denan Wang,[§] Adam T. Fiedler,*[,§] and Justin R. Walensky*[,†]

[†]Department of Chemistry, University of Missouri, 601 S. College Avenue, Columbia, Missouri 65211, United States

[‡]Department of Biophysics, Medical College of Wisconsin, 8701 Watertown Plank Road, Milwaukee, Wisconsin 53226, United States

[§]Department of Chemistry, Marquette University, 535 North 14th Street, Milwaukee, Wisconsin 53233, United States

Supporting Information

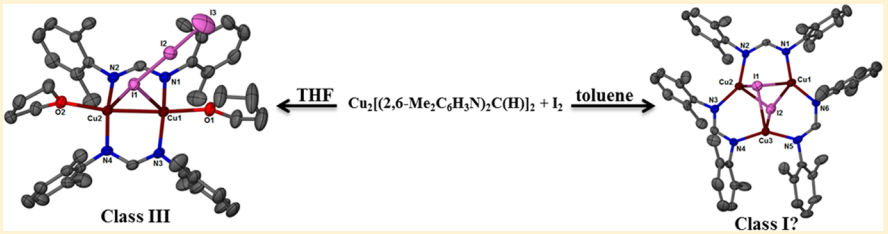

ABSTRACT: Molecular examples of mixed-valence copper complexes through chemical oxidation are rare but invoked in the mechanism of substrate activation, especially oxygen, in copper-containing enzymes. To examine the cooperative chemistry between two metals in close proximity to each other we began studying the reactivity of a dinuclear Cu(I) amidinate complex. The reaction of $[(2,6\text{-}Me_2C_6H_3N)_2C(H)]_2Cu_2$, **1**, with I_2 in tetrahydrofuran (THF), CH_3CN, and toluene affords three new mixed-valence copper complexes $[(2,6\text{-}Me_2C_6H_3N)_2C(H)]_2Cu_2(\mu_2\text{-}I_3)(THF)_2$, **2**, $[(2,6\text{-}Me_2C_6H_3N)_2C(H)]_2Cu_2(\mu_2\text{-}I)(NCMe)_2$, **3**, and $[(2,6\text{-}Me_2C_6H_3N)_2C(H)]_3Cu_3(\mu_3\text{-}I)_2$, **4**, respectively. The first two compounds were characterized by UV−vis and electron paramagnetic resonance spectroscopies, and their molecular structure was determined by X-ray crystallography. Both di- and trinuclear mixed-valence intermediates were characterized for the reaction of compound **1** to compound **4**, and the molecular structure of **4** was determined by X-ray crystallography. The electronic structure of each of these complexes was also investigated using density functional theory.

INTRODUCTION

Copper-containing enzymes play a central role in the activation of small molecules such as O_2 and N_2O;[1] hence, elucidating new possibilities for metal-mediated small molecule activation through synthetic models is one approach to understanding their enzymatic activity. Even though a mixed-valence state is invoked in the mechanism of several copper-containing enzymes such as nitrous oxide reductase,[2,3] cytochrome *c* oxidase,[4,5] and hemocyanin,[6] few molecular examples of mixed-valence copper complexes have been isolated. Synthetically, this is typically done by self-assembly,[7−22] electrochemically,[23,24] and, less commonly, by chemical redox.[25−32] Additionally, mixed-valence Cu coordination polymers are prevalent.[33−36] The use of nitrogen-donor ligands for modeling Cu-containing enyzmes is well-established leading to mechanistic details, especially for monometallic copper complexes.[37] For example, the interaction of Cu(I) and O_2 with β-diketiminate ligands has been shown to involve an oxidation of Cu(I) to Cu(II) with concomitant one-electron reduction of O_2 to the superoxide O_2^-.[38] Finally, the Karlin group has many examples of O_2 activation with dinuclear Cu(I) complexes for modeling multinuclear copper clusters that catalyze oxidase reactions.[39]

The Cu_A site of cytochrome *c* oxidase contains two four-coordinate copper ions, bridging dithiolates, ∼2.6 Å apart, and has mixed-valence 2Cu(1.5,1.5) resting state. Copper(I) amidinate complexes[40,41] feature two copper(I) ions with a similar Cu−Cu separation and have two nitrogen atoms coordinated similar to the Cu_A site, which has a nitrogen from histidine coordinated to each copper, Figure 1. The reactivity of bimetallic Cu(I) amidinate complexes is virtually unknown, and our objective was to expand on the chemistry of a dinuclear Cu(I) complex, $[(2,6\text{-}Me_2C_6H_3N)_2C(H)]_2Cu_2$, **1**, we recently reported.[42] One mixed-valence copper amidinate complex has been reported.[7f] On the basis of **1**, we herein report the synthesis and characterization of three new mixed-valence copper complexes simply from reactivity differences in polar (tetrahydrofuran (THF) and $NCCH_3$) and nonpolar (toluene) solvents. The reactions with **1** and I_2 in THF and $NCCH_3$ have similar electronic structure to the Cu_A site.

Received: May 27, 2015
Published: August 7, 2015

DOI: 10.1021/acs.inorgchem.5b01161
Inorg. Chem. 2015, 54, 8509−8517

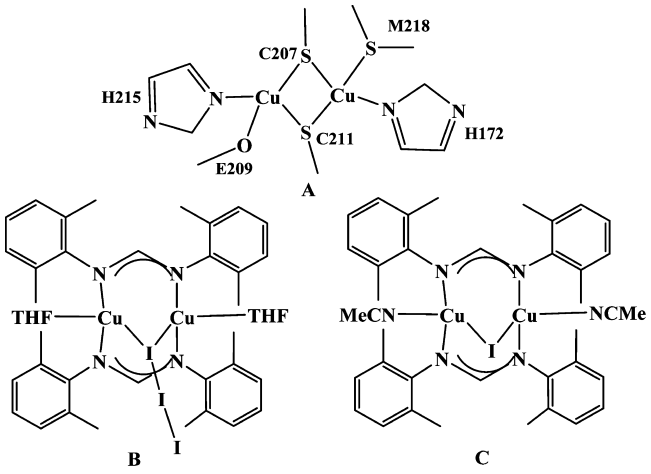

Figure 1. (A) Rudimentary illustration of Cu_A site of cytochrome *c* oxidase. (B, C) Mixed-valence copper amidinate complexes presented in this work.

EXPERIMENTAL SECTION

General Considerations. All manipulations were performed inside an argon or nitrogen atmosphere Vacuum Atmosphere OMNI glovebox with rigorous exclusion of air and water unless otherwise specified. Anhydrous solvents (Aldrich) were purchased, sparged with nitrogen, and stored over molecular sieves. $[Cu(NCMe)_4]PF_6$ (Strem) was used as received. I_2 (Aldrich) was sublimed prior to use. $Cu_2[(2,6\text{-}Me_2C_6H_3N)_2C(H)]_2$, **1**, was synthesized as previously reported.[42] Fourier transform infrared measurements were made on a Thermo-Nicolet instrument using spectroscopic grade KBr. The UV−vis−near-IR measurements were collected with a Cary 5000 instrument. Solid-state Raman measurements were obtained on a Renishaw InVia spectrometer at an excitation wavelength of 632.8 nm. Elemental analysis was performed by Atlantic Microlab, Inc. (Norcross, GA).

Synthesis of $[(2,6\text{-}Me_2C_6H_3N)_2C(H)]_2Cu_2(\mu_2\text{-}I_3)(THF)_2$, 2. In a scintillation vial, **1** (100 mg, 0.16 mmol) was dissolved in THF (10 mL), and I_2 (40 mg, 0.16 mmol) was added at room temperature. The solution color immediately changed from colorless to dark brown-red. After 4 h, the solvent was removed under vacuum to yield a dark brown-red powder (90 mg, 56%). Anal. Calcd For $Cu_2C_{42}H_{54}I_3N_4O_2$: C, 43.69%; H, 4.71%; N, 4.85%. Found: C, 43.65%; H, 4.32%; N, 4.69%. X-ray quality crystals were grown overnight from a saturated THF solution at −25 °C. UV−vis−NIR (0.97 mM, THF): 530 nm (ε = 2250 M^{-1} cm^{-1}), 1100 nm (ε = 200 M^{-1} cm^{-1}), 1940 nm (ε = 500 M^{-1} cm^{-1}). IR (KBr): 3321 (w), 2966 (w), 2908 (w), 2157 (s), 1646 (s), 1585 (m), 1458 (m), 1298 (m), 1184 (m), 1086 (m), 755 (m).

Synthesis of $[(2,6\text{-}Me_2C_6H_3N)_2C(H)]_2Cu_2(\mu_2\text{-}I)(NCMe)_2$, 3. In a scintillation vial, **1** (100 mg, 0.16 mmol) was dissolved in acetonitrile (15 mL), and I_2 (40 mg, 0.16 mmol) was added at room temperature. The solution color immediately changed from colorless to dark red. After 4 h, the solvent was removed under vacuum to yield a dark red-brown powder (96 mg, 71%). Anal. Calcd for $Cu_2C_{38}H_{44}IN_6$: C, 54.41%; H, 5.29%; N, 10.02%. Found: C, 54.25%; H, 5.37%; N, 9.88%. X-ray quality crystals were grown overnight from a saturated acetonitrile solution at −25 °C. UV−vis−NIR (0.88 mM, $NCCH_3$): 500 (sh) nm (1600 M^{-1} cm^{-1}), 860 nm (ε = 500 M^{-1} cm^{-1}), 1510 nm (ε = 250 M^{-1} cm^{-1}). IR (KBr): 3051 (w), 2937 (w), 2908 (w), 2153 (m), 1638 (m), 1564 (s), 1470 (s), 1323 (s), 1254 (m), 1196 (s), 1089 (m), 767 (s).

Synthesis of $[(2,6\text{-}Me_2C_6H_3N)_2C(H)]_3Cu_3(\mu_3\text{-}I)_2$, 4. In a scintillation vial, **1** (100 mg, 0.16 mmol) was dissolved in toluene (10 mL), and I_2 (40 mg, 0.16 mmol) was added at room temperature. The solution color immediately changed from colorless to dark brown-red. After 4 h, the solvent was removed under vacuum to yield a dark brown powder (96 mg, 50%). Anal. Calcd for $Cu_3C_{58}H_{65}I_2N_6$: C, 53.98%; H, 5.08%; N, 6.51%. Found: C, 54.37%; H, 4.75%; N, 6.34%. X-ray quality crystals were grown overnight from a saturated toluene solution at −25 °C. UV−vis−NIR (1.05 mM, toluene): 480 (sh) nm (ε = 1000 M^{-1} cm^{-1}), 680 nm (ε = 250 M^{-1} cm^{-1}). IR (KBr): 3019 (w), 2944 (m), 2914 (m), 2155 (m), 1646 (m), 1564 (m) 1467 (m), 1194 (m), 1091 (m), 1029 (w), 763 (m).

Crystal Structure Determination and Refinement. The selected single crystals of **2**−**4** were mounted on a nylon cryoloop using viscous hydrocarbon oil. X-ray data collection was performed at 100(2) or 173(2) K. The X-ray data were collected on a Bruker CCD diffractometer with monochromated Mo Kα radiation (λ = 0.710 73 Å). The data collection and processing utilized Bruker Apex2 suite of programs.[43] The structures were solved using direct methods and refined by full-matrix least-squares methods on F^2 using Bruker SHELX-97 program.[44] All non-hydrogen atoms were refined with anisotropic displacement parameters. All hydrogen atoms were placed at calculated positions and included in the refinement using a riding model. Thermal ellipsoid plots were prepared by using X-seed[45] with 30 or 50% of probability displacements for non-hydrogen atoms. Crystal data and details for data collection for complexes **2**−**4** are also provided in Table 1.

Table 1. X-ray Crystallographic Data for Complexes 2−4

	2·2THF	3	4·C_7H_8
CCDC deposit number	893748	1400878	893747
empirical formula	$Cu_2C_{50}H_{70}I_3N_4O_4$	$Cu_2C_{38}H_{44}IN_6$	$Cu_3C_{58}H_{65}I_2N_6$
formula weight (g/mol)	1298.88	838.77	1290.58
crystal habit, color	plate, brown-red	plate, red	plate, brown-purple
temperature (K)	173(2)	100(2)	173(2)
space group	$P2_1/n$	$P2_1/c$	$Pna2_1$
crystal system	monoclinic	monoclinic	orthorhombic
volume (Å^3)	5300.3(5)	3736.1(6)	5475.2(17)
a (Å)	11.0680(6)	10.9071(10)	26.456(5)
b (Å)	15.4780(8)	22.984(2)	24.908(5)
c (Å)	30.9839(17)	15.0298(13)	8.3089(15)
α (deg)	90	90	90
β (deg)	93.0530(10)	97.4430(10)	90
γ (deg)	90	90	90
Z	4	4	4
calculated density (Mg/m^3)	1.628	1.491	1.566
absorption coefficient (mm^{-1})	2.594	1.999	2.325
final *R* indices [$I > 2\sigma(I)$]	*R*1 = 0.0392, *w*R2 = 0.0485	*R*1 = 0.0218, *w*R2 = 0.0522	*R*1 = 0.0473, *w*R2 = 0.0928

Electron Paramagnetic Resonance Spectroscopy. Most X-band electron paramagnetic resonance (EPR) spectra at 110 K were obtained with a Bruker EMX spectrometer located at the National Biomedical EPR Center at the Medical College of Wisconsin. Spectra were simulated with EasySpin.[46] Additional X-band spectra were obtained at 10 K with an Elexsys E500 EPR spectrometer, Bruker, Billerica, MA. Q-band spectra were obtained on a Varian E109 spectrometer. Low-frequency spectra (S-band (3.5 GHz) and L-band (2.0 GHz)) were obtained using home-built bridges and resonators at the National Biomedical EPR Center.

Density Functional Theory Calculations. These calculations were performed using the ORCA 2.9 software package developed by Neese (MPI for Chemical Energy Conversion).[47] The computational models were derived from the crystallographic coordinates, although the methyl substituents at the 2- and 6-positions of the phenyl rings were replaced by hydrogen atoms, which were added by assuming idealized C−H bond lengths and angles. The calculations utilized

DOI: 10.1021/acs.inorgchem.5b01161
Inorg. Chem. 2015, 54, 8509−8517

Becke's three-parameter hybrid functional for exchange along with the Lee–Yang–Parr correlation functional (B3LYP).[48,49] Ahlrichs' valence triple-ζ basis set (TZV), in conjunction with the TZV/J auxiliary basis set,[50,51] were used for the nonmetallic atoms; the "core properties" with extended polarization [CP(PPP)] basis set[52] was used for the Cu atoms. The contribution of spin–orbit coupling to the **g** and **A** tensors was evaluated by solving the coupled-perturbed self-consistent field (CP-SCF) equations.[53−56] To ensure the accuracy of the hyperfine coupling constants, a high-resolution grid with an integration accuracy of 7.0 was generated for the Cu atoms. Isosurface plots of molecular orbitals were prepared with the gOpenMol program[57] developed by Laaksonen. Time-dependent density functional theory (TD-DFT) calculations[58−60] computed absorption energies and intensities using the Tamm–Dancoff approximation.[61,62]

RESULTS AND DISCUSSION

We began exploring the reactivity of **1** to compare with the Au(I) analogue, that is, $Au_2(amid)_2$.[63] While the reaction of $Au_2(amid)_2$ with I_2 produced a green product, $Au_2(amid)_2I_2$, containing two Au(II) centers, **1** with I_2 in THF produces a dark red-brown solution, eq 1. The ^{1}H NMR spectrum showed

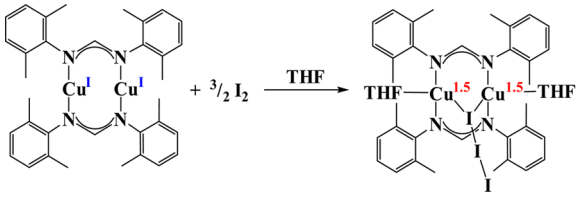

(1)

broad resonances indicating a paramagnetic species, but no other conclusions could be drawn. The UV–vis–NIR spectrum showed an absorption in the visible region at 530 nm (Figure S1). Absorptions at 1100 and 1940 nm were observed for **2** in the near-IR region (Figure S1). Dark red-brown crystals suitable for X-ray crystallography analysis were obtained from a saturated THF solution at −35 °C definitively identifying the product as $[(2,6\text{-}Me_2C_6H_3N)_2C(H)]_2Cu_2(\mu_2\text{-}I_3)(THF)_2$, **2**, Figure 1. Complex **2** is the one-electron reduction of I_2 to I_3^-, which bridges the two Cu metals, and one THF solvent molecule coordinates to each metal as well. On the basis of formal valence, one metal must be Cu(I) and the other Cu(II).

The structure of **2**, Figure 2, shows a similar structure to the parent compound, **1**, with each Cu coordinated to the nitrogen of the same amidinate ligand. The Cu1–N1 and Cu1–N4 bond distances of 1.915(4) and 1.916(4) Å are slightly longer than the 1.904(4) and 1.910(4) Å lengths of Cu2–N2 and Cu2–N3. The metal–metal bond is now 2.5103(9) Å, which is shorter than 2.5477(14) Å in **1**.

One remarkable feature of **2** is the bridging triiodide ligand, as we can find no previous reports of this common counteranion behaving as an η^1-bridging ligand between two metal centers. Reports of I_3^- as a terminal[64−70] and bridging ligand have been described but with one metal bound η^1 to both terminal iodine atoms.[71,72] The solid-state Raman spectrum of **2** gave absorption at 168 cm^{-1}, indicative of the triiodide ligand, Figure S2.

The electronic structure of **2** was probed using EPR spectroscopy. The X-band spectrum of **2**, Figure 3, is well-resolved about the high-field *g*-value, g_z, where A_z = 78 G in a 1:2:3:4:3:2:1 pattern, where the last four lines are separated from the rest of the spectrum, and the intensities of the last four high-field lines fit the pattern. The first harmonic spectrum, Figure 3, emphasizes some of the low-field lines. A well-fit spectral simulation gives insight into the EPR parameters. To

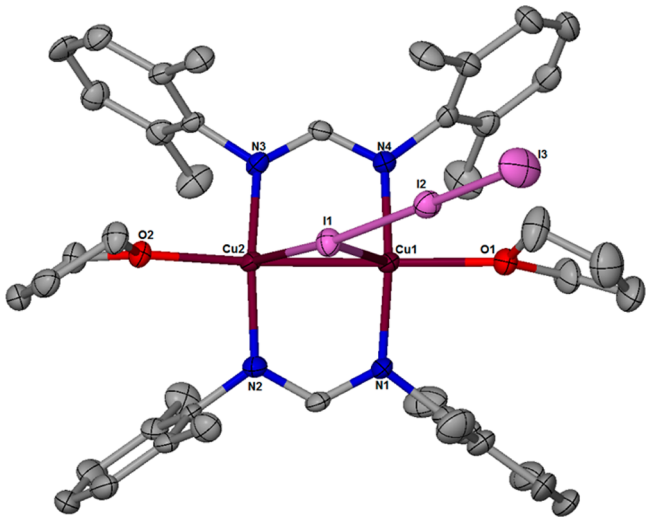

Figure 2. Molecular structure of **2**·2THF with thermal ellipsoids projected at 50% probability level. Hydrogen atoms and solvent molecules were omitted for clarity. Selected bond distances (Å) and angles (deg): Cu1–N1:1.915(4); Cu1–N4:1.916(4); Cu1–I1:2.9991(9); Cu1–O1:2.167(4); Cu1–Cu2:2.5103(9); Cu2–N2:1.904(4); Cu2–N3:1.910(4); Cu2–O2:2.127(4); Cu1–I1–Cu2:48.458(18); N1–Cu1–N4:159.1(2); N1–Cu1–O1:94.52(17); N3–Cu2–N2:160.58(19); N2–Cu2–O2:94.82(17).

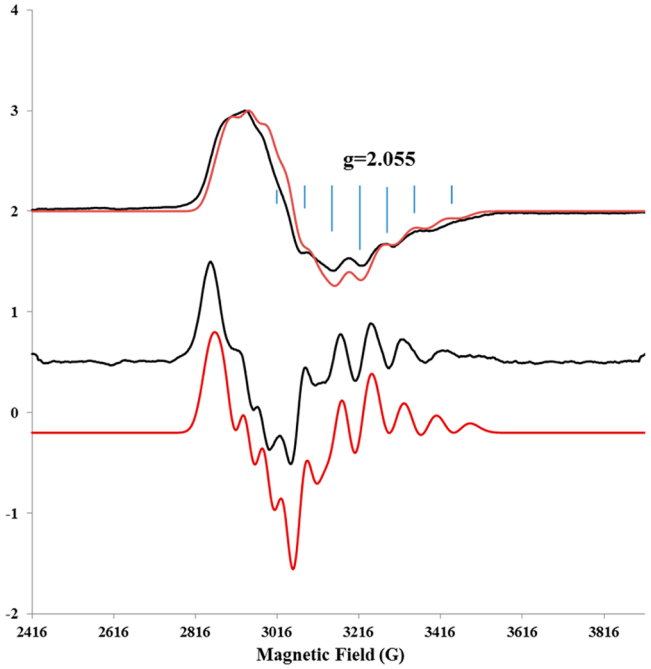

Figure 3. X-band spectrum of **2** in THF at 110 K: Expt (black traces, 1st harmonic 2% Bessel); Siml (red traces) g = 2.220, 2.170, 2.055; A = 120, 140, 218 MHz (43, 50, 78 G); lwpp 5 G, HStrain 160 150 180, microwave freq 9.292 GHz.

confirm that the g_z value is centered in the middle of the seven-line pattern for a dinuclear copper species and not a 10-line pattern for a trinuclear copper complex, the *g*-values, 2.209, 2.158, and 2.053, were obtained at Q-band, 34.81 GHz, where the *g*-values are better separated (Figure S3). This confirms that the *g*-value on the high field side is a seven-line pattern due to a mixed-valence dinuclear 2Cu(1.5,1.5) complex.[73,74] Therefore, **2** is a Class III species.[75] At lower microwave frequencies, the

DOI: 10.1021/acs.inorgchem.5b01161
Inorg. Chem. 2015, 54, 8509–8517

low-field side of the spectrum is better resolved, but the g_z region is less-resolved than at X-band.

The electronic structure and spectroscopic features of complex **2** were further probed using DFT. These calculations employed the hybrid B3LYP functional and the crystallographically determined structure, although the methyl substituents of the phenyl rings were replaced with H atoms. The computed singly occupied molecular orbital (SOMO), shown in Figure 4, is best described as the antibonding combination of

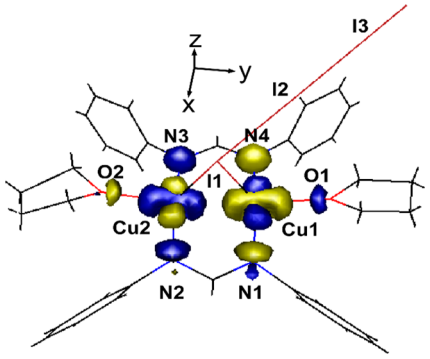

Figure 4. DFT-generated isosurface plot of the SOMO of complex **2**. The orientation of the **g**-tensor is indicated by the coordinate system; by convention, the *x*-axis is assigned to g_{min}, and the *z*-axis is assigned to g_{max}.

the two Cu-based d(x^2-y^2) orbitals, consistent with the shortening of the Cu−Cu interaction upon oxidation. The overall composition of the SOMO is 39% Cu1, 31% Cu2, and 14% N_{amid}, with only minor contributions from the THF (4%) and I_3^- (2%) ligands. For reference, the estimated spin-density distribution in the Cu_A site has been calculated to be 38%.[76] Thus, the unpaired electron is almost evenly delocalized over the two copper centers, also consistent with the assignment of **2** as a class III mixed-valence compound.

As summarized in Table S1, the *g*-values of 2.200, 2.152, and 2.066 provided by DFT are quite close to the experimental values determined by EPR spectroscopy. We also computed hyperfine coupling values for the two Cu nuclei, and both **A**-tensors feature large contributions from spin-dipolar and spin−orbit coupling terms. The ^{63}Cu **A**-tensors are not coincident with each other, or with the molecular **g**-tensor (Table S1). Therefore, it was necessary to simulate the predicted EPR spectrum using the Euler angles provided by the calculation, and the results are shown in Figure 5. Since the magnitudes of the computed *A*-values are approximately the same for the two nuclei, each EPR feature displays a seven-line pattern (although such splitting may not be resolved in the actual spectrum). In good agreement with the experimental data, DFT predicts a hyperfine splitting of 234 MHz for the high-field g_x resonance and smaller *A*-values of 85 and 180 MHz for the g_y and g_z features, respectively (Figure 5). Collectively, these DFT calculations nicely reproduce the distinctive spectroscopic features of complex **2**.

Performing the reaction of **1** with I_2 in acetonitrile affords a dark red colored solution, eq 2. The UV−vis−NIR spectrum of **3** (Figure S1) showed different absorptions to **2**, indicating the formation of a new species. Complex **3** has one shoulder feature around 500 nm and two NIR absorptions at 860 and 1510 nm. The feature at 860 nm is similar to that for the Cu_A site at 808 nm.[77] The absorption spectra of **2** and **3** were

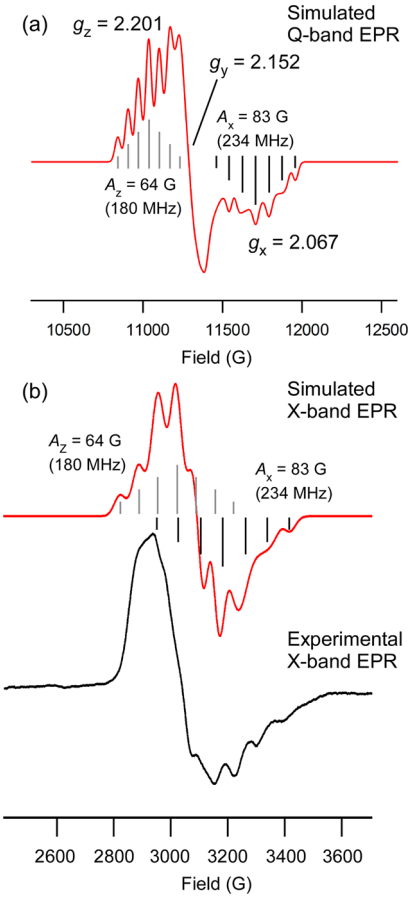

Figure 5. Simulated EPR spectra of complex **2** generated with DFT-calculated parameters. The microwave frequency employed in the simulations was either 34.0 (a) or 9.28 (b) MHz. The experimental X-band EPR spectrum is shown at the bottom.

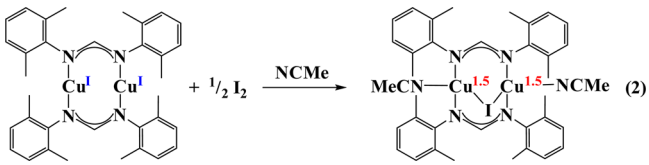

interpreted with the aid of TD-DFT calculations. For both complexes, the computed spectra (Figure S4) nicely reproduce the presence of broad features in the NIR region between 800 and 2000 nm. DFT attributes these NIR bands to charge-transfer (CT) transitions from the I_3^- (or I^-) ligand to the $[Cu_2]^{3+}$ unit. These bands are rather weak ($\varepsilon \approx 1000$ M^{-1} cm^{-1}) due to poor overlap between I_3^- (or I^-)-based orbitals and the Cu-based SOMO. The intervalence CT transition is predicted by TD-DFT to occur at 466 nm for **2** and 475 nm for **3**, corresponding to the experimentally observed bands at 530 and 500 nm, respectively.

Dark red crystals were obtained from a saturated acetonitrile solution at −25 °C, and the structure was determined as $[(2,6\text{-}Me_2C_6H_3N)_2C(H)]_2Cu_2(\mu_2\text{-}I)(NCCH_3)_2$, **3**, Figure 6. Complex **3**, in analogy to **2**, has coordinated solvent molecules, in this case acetonitrile. Interestingly, only an iodide remains that bridges each copper ion. In addition, the Cu−Cu bond distance is 2.4810(3) Å, ∼0.06 Å decrease from **1** and 0.03 Å from **2**. The difference between **2** and **3** and a previously reported mixed-valence Cu(1.5,1.5) complex is in Lee's complex,

DOI: 10.1021/acs.inorgchem.5b01161
Inorg. Chem. 2015, 54, 8509−8517

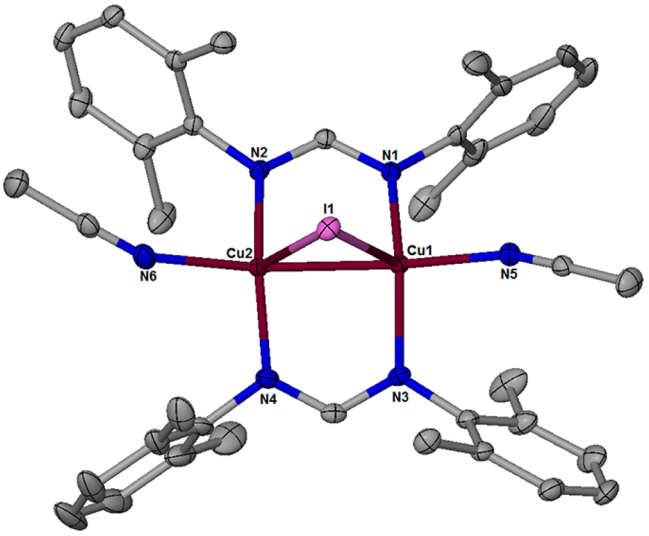

Figure 6. Molecular structure of **3** with thermal ellipsoids projected at 50% probability level. Hydrogen atoms were omitted for clarity. Selected bond distances (Å) and angles (deg): Cu1−N1:1.9257(15); Cu1−N3:1.9409(15); Cu1−N5:2.0533(16); Cu1−I1:2.8276(3); Cu2−N2:1.9475(15); Cu2−N4:1.9387(15); Cu2−N6:2.0790(17); Cu1−Cu2:2.4810(3); Cu1−I1−Cu2:52.245(8); N1−Cu1−N3:146.21(6); N3−Cu1−N5:95.25(6); N2−Cu2−N4:147.25(6); N4−Cu2−N6:93.42(6).

$\{Cu_2[2,6\text{-}Me_2C_6H_3N)_2C(Ph)]_2\}^+$,[7f] where the backbone carbon atom has a phenyl group in the amidinate ligand, and **2** and **3** are neutral instead of cationic as well as contain triiodide or iodide. The molecular and electronic structures of **2**, **3**, and $\{Cu_2[2,6\text{-}Me_2C_6H_3N)_2C(Ph)]_2\}^+$ are similar in their bond metrics and similar spectroscopic features. The more sterically crowded amidinate complex bearing the phenyl group shows shorter Cu−Cu bond distances of an average of 2.42(1) Å between two independent molecules in the unit cell for the THF adduct and 2.4571(2) Å between two independent molecules for the acetonitrile-coordinated complex.

The X-band EPR spectrum for the reaction in acetonitrile, Figure 7, is resolved on both the high- and low-field sides of the spectrum where a simulation of the spectrum and the first harmonic (derivative) gives *g*-values of 2.23, 2.14, and 2.04 and *A*-values of 60, 36, and 61 G.

DFT calculations of complex **3** also converge to a class III mixed-valence ground state in which the unpaired spin density is fully delocalized over the two Cu centers. The composition of the SOMO is 34% Cu1, 34% Cu2, and 15% N_{amid}, with minimal contributions from other moieties. The computed *g*-values of 2.187, 2.151, and 2.066 adequately mimic the experimental values, although DFT underestimates the rhombicity of the molecular **g** tensor. As in the case of complex **2**, the **A** tensors of the two Cu nuclei adopt different orientations than the **g** tensor, necessitating the use of Euler angles. The simulated EPR spectra, shown in Figure S5, exhibit hyperfine splittings of 160, 60, and 220 MHz for A_x, A_y, and A_z, respectively. These values are consistent with the experimental EPR studies, which found large *A*-values of ∼170 MHz in the high- and low-field features.

When the reaction of **1** with I_2 is performed in toluene a dark purple-brown solution, eq 3, was observed with only one absorbance at 495 nm in the visible region (Figure S1). The UV−vis−NIR spectrum revealed two features in the visible region at 480 and 680 nm and no absorptions in the NIR

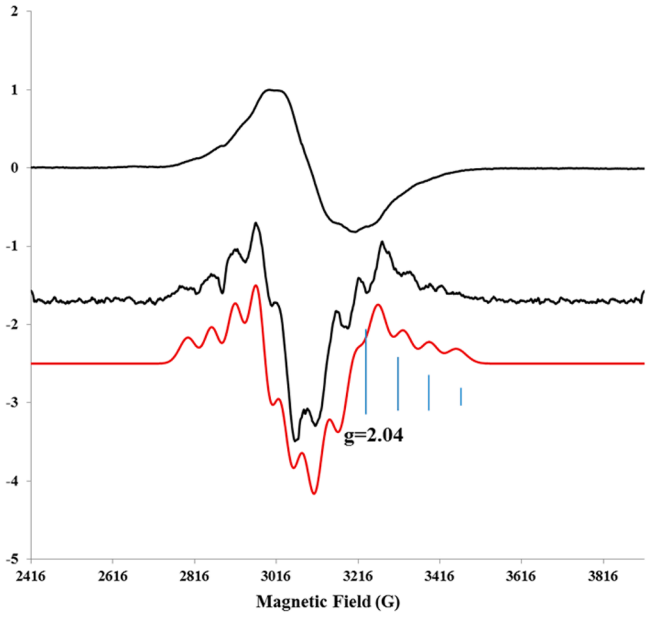

Figure 7. X-band spectrum of **3** in acetonitrile: Expt (black traces, 1st harmonic 2% Bessel) microwave freq 9.282 GHz, microwave power 16 dB (5 mW), 9 scans, mod. Amp. 5 G, temperature 110 K; Siml (red trace): g = 2.23, 2.14, 2.04, A = 167, 100, 170 MHz (60 36 61 G), line width peak to peak 5 G, Hstrain 150 200 170. Vertical lines indicate four of the seven line pattern on the high-field side.

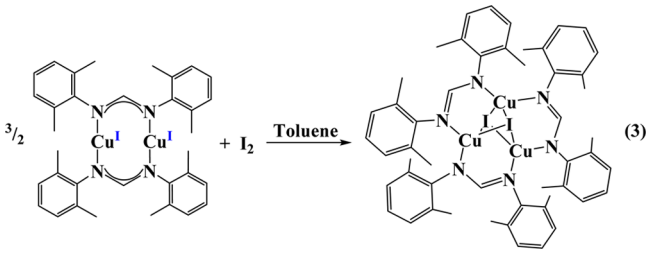

(3)

region. Crystals suitable for X-ray diffraction determined the structure as $[(2,6\text{-}Me_2C_6H_3N)_2C(H)]_3Cu_3(I)_2$, **4**, a trinuclear product, Figure 8. In this case, for a neutral complex there must be two Cu(II) ions and one Cu(I). This was also evidenced by an S = 1 ground state as established using Evans' method.

The structure of **4** resembles the mixed-valence 3Cu-(II,III,III) complex isolated by the Stack group from O_2 activation; however, **4** contains iodide ions instead of oxo groups.[78] Each Cu ion is four-coordinate in a pseudotetrahedral geometry consisting of two nitrogen atoms, one from a different amidinate as is seen in **1**, and two individual iodide atoms. The N1−Cu1−N6 bond angle is more obtuse than an ideal tetrahedron at 141.3(2)°; however, the N1−Cu1−I1, N6−Cu1−I2, and I1−Cu1−I2 angles are 101.94(18), 103.46(18), and 101.88(3)°, respectively. Note that the I1−I2 separation is 4.376 Å, so these are two distinct iodide ions. The Cu−I bond distances showed those to Cu3 to be elongated at 3.0645(11) and 2.8085(11) Å compared to Cu1, 2.6416(12) and 2.9870(12) Å, and Cu2, 2.7956(11) and 2.6667(12) Å.

While the EPR spectra for **2** and **3** were straightforward, the spectrum for **4** was complicated. Spectra were taken at different time intervals, and the results varied with increasing time. In the first 2 h, spectra appear similar to those found for **2**, Figure 9, with nicely resolved seven-line patterns indicating that the

DOI: 10.1021/acs.inorgchem.5b01161
Inorg. Chem. 2015, 54, 8509−8517

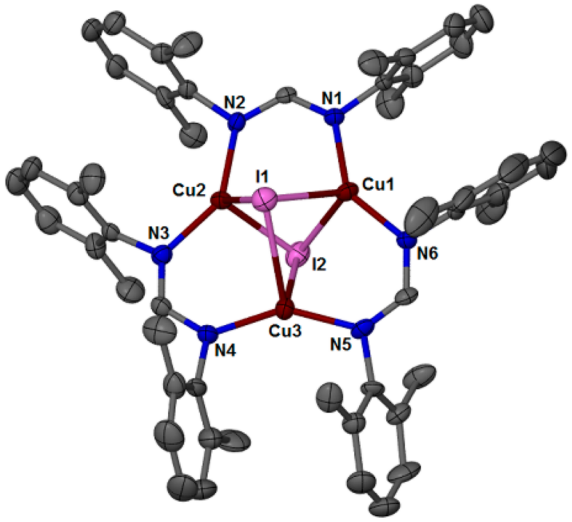

Figure 8. Molecular structure of $4{\cdot}C_7H_8$ with thermal ellipsoids projected at 50% level. Hydrogen atoms and solvent molecule were omitted for clarity. Selected bond distances (Å) and angles (deg): Cu1–N1:1.927(5); Cu1–N6:1.890(6); Cu2–N2:1.912(5); Cu2–N3:1.899(6); Cu3–N4:1.909(6); Cu3–N5:1.917(6); Cu1–I1:2.6416(12); Cu2–I1:2.7956(11); Cu3–I1:3.0645(11); Cu1–I2:2.9870(12); Cu2–I2:2.6667(12); Cu3–I2:2.8085(11); Cu1–I1–Cu2:68.81(3); Cu1–I1–Cu3:65.58(3); N1–Cu1–N6:141.3(2); N6–Cu1–I1:106.97(18); N1–Cu1–I2:95.01(18); N1–Cu1–I1:101.94(18); N6–Cu1–I2:103.46(18); I1–Cu1–I2:101.88(3).

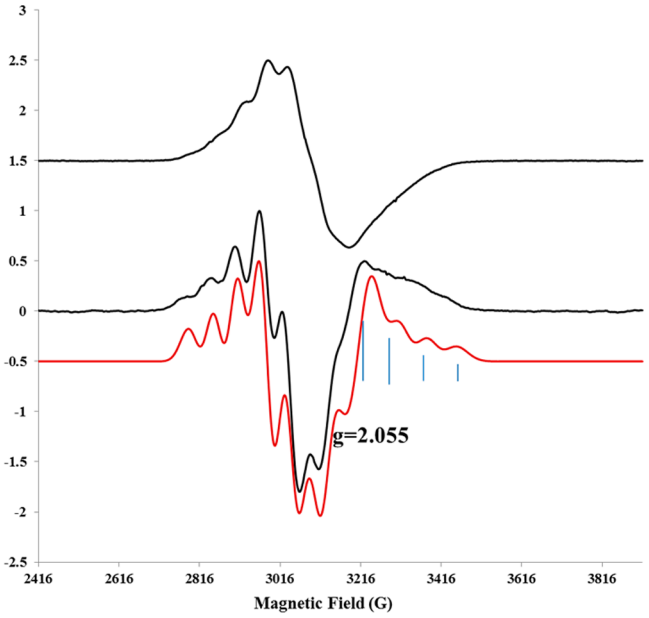

Figure 9. X-band EPR spectra in toluene of an intermediate preceding **4** indicative of two copper ions with $S = 1/2$. Experimental spectra (black traces, 1st harmonic (2% Bessel); microwave freq 9.282 GHz; microwave power 16 dB (5 mW); 9 scans, mod amp 5 G; temperature 110 K; Simulation (red trace) g = 2.22, 2.14, 2.055; A = 177, 90, 190 MHz (63, 32, 68 G); line withdth peak to peak 5 G; HStrain 150 200 170. Vertical lines indicate four of the seven line pattern for the high-field g-value.

initial reaction of **1** with I_2 in toluene also proceeds through a dinuclear, mixed-valence species. If the reaction is spiked with THF, **2** is obtained. Between 2 and 8 h, the spectrum changes to a trinuclear complex due to the presence of 10-line pattern in the EPR spectrum, Figure 10. However, this is not the EPR spectrum of **4** as the spin state is $S = 1/2$ not 1. The spectrum

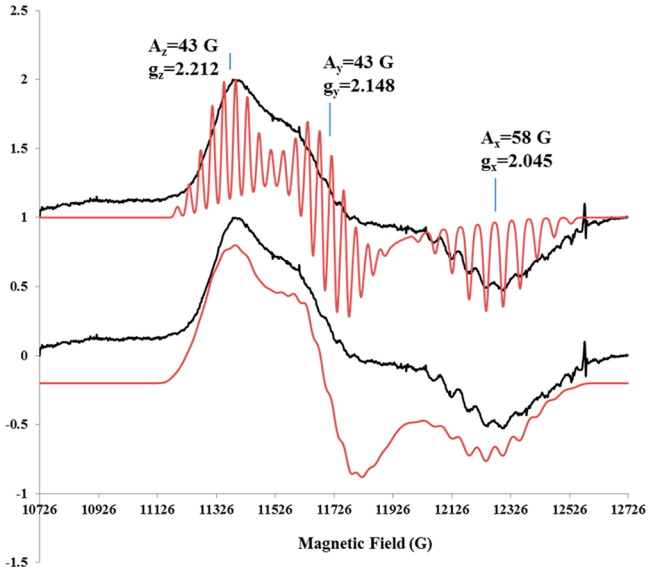

Figure 10. Q-band EPR spectrum in toluene of an intermediate three-copper mixed-valence compound preceding **4** indicating three copper centers with $S = 1/2$. Experimental spectra (black traces), microwave frequency 34.768 GHz; temperature 10 K; 9 scans; mod amp 5 G; power 22 dB; time constant 0.1 s; scan time 2 min. Simulated spectra (red traces) HStrain 50 50 50 (upper); 150 130 150 (lower).

was simulated with g-values 2.212, 2.148, and 2.045. Some copper hyperfine is resolved for the middle g-value, but the best resolution is for the high-field g-value. The best-resolved Q-band spectrum for the intermediate leading to **4** in toluene, which is simulated with a 10-line pattern (1:3:6:10:12:12:10:6:3:1), has an A_x value of 58 G, Figure 10. The best-resolved Q-band spectrum for a mixed-valence two copper intermediate leading to **4** in toluene, which is simulated with a seven-line pattern (1:2:3:4:3:2:1), has an A_x value of 77 G, Figure S6. The loss of resolution throughout the other spectra and the poorly resolved lines for A_z are attributed to a mixture of dinuclear and trinuclear complexes having superimposed spectra. Finally, after 8 h, no EPR spectrum can be obtained, and the complex is EPR silent.

While the mechanism of the formation of **4** is unknown, some deductions can be made from the EPR spectra. The EPR spectrum, Figure 9 and Figure S3, in the first 2 h is similar to those of **2** and **3** indicating that a dinuclear 2Cu(1.5,1.5) intermediate species is formed with a structure similar to that of **2** or **3**. In THF or acetonitrile, those adducts flank each copper ion and provide the further electron density that is necessary to accommodate the increased Lewis acidity of the copper upon oxidation. However, in toluene, the first intermediate complex that forms is similar, but since solvent molecules are not available to coordinate to copper, the complex rearranges to form a trinuclear copper species. Still, only one reduction has taken place. This is supported by Figure 10. Once the intermediate trinuclear copper complex is assembled, the trinuclear, $S = {}^1/_2$ complex oxidizes a second time to produce **4**. This is outlined in Scheme 1. Since **4** is a non-Kramer state ($S = 1$), **4** is EPR silent, presumably due to the large zero-field splitting (ZFS).

DOI: 10.1021/acs.inorgchem.5b01161
Inorg. Chem. 2015, 54, 8509–8517

Scheme 1. Proposed Formation of 4

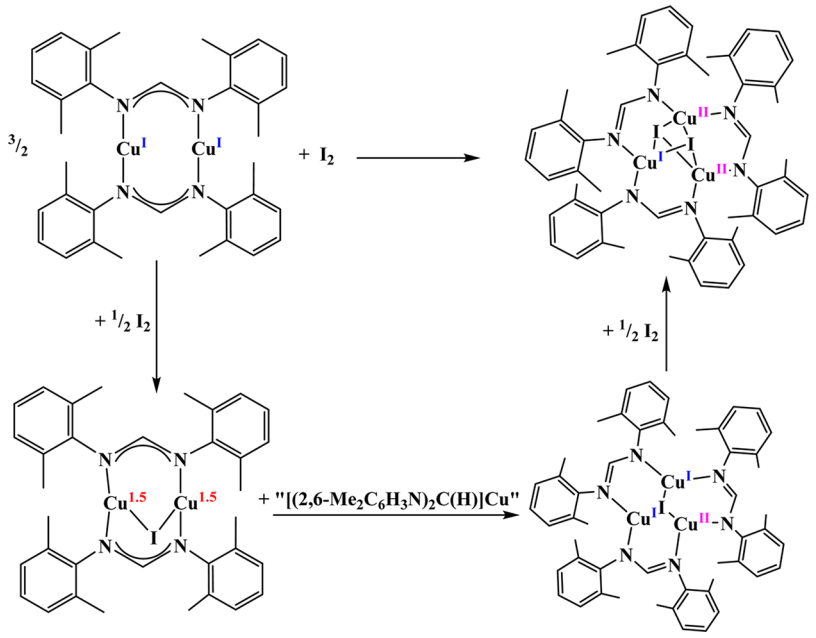

DFT calculations aided in the identification of oxidation states in the tricopper complex **4**. These calculations employed the crystallographic structure and assumed an $S = 1$ ground state. The SOMOs in complex **4** are strongly delocalized over the entire $[Cu_3I_2]^{3+}$ unit, making it difficult to assign oxidation states with confidence. However, the computed Mulliken spins indicate that Cu1 and Cu2 possess a sizable amount of unpaired spin density (0.36 and 0.48 spins, respectively), while substantially less spin density is localized on Cu3 (0.14 spins). It therefore appears that Cu1 and Cu2 are cupric (+2), while Cu3 is the lone cuprous (+1) ion. This conclusion is consistent with the relative Cu−I bond lengths observed in the crystal structure. This is a rare example of a trinuclear copper complex with two cupric ions and one cuprous ion,[79] and the other Cu(I,II,II) compound was also EPR silent. In Tolman's Cu(I,II,I) compound,[80] an EPR spectrum could be achieved indicating a Class I species. The Murray group has recently reported a trinuclear copper complex, which was also difficult to classify, and it is possible that **4** has a similar electronic structure.[81]

CONCLUSION

We have demonstrated the facile synthesis of mixed-valence 2Cu(1.5,1.5) complexes using a dinuclear Cu(I) amidinate starting material and I_2 reduction. These complexes were each obtained using the same reaction conditions except different solvents. In THF and acetonitrile, dinuclear products were obtained; respectively, they were $[(2,6\text{-}Me_2C_6H_3N)_2C(H)]_2Cu_2(\mu_2\text{-}I_3)(THF)_2$, **2**, and $[(2,6\text{-}Me_2C_6H_3N)_2C(H)]_2Cu_2(\mu_2\text{-}I)(NCCH_3)_2$, **3**. However, in toluene, mixed-valence di- and trimetallic intermediate compounds were detected by EPR spectroscopy, and a trinuclear compound, $[(2,6\text{-}Me_2C_6H_3N)_2C(H)]_3Cu_3(\mu_3\text{-}I)_2$, **4**, was isolated. Despite I_2 not being a biologically relevant substrate with respect to copper-containing enzymes, the use of an inorganic substrate to gain insight into biomimetic chemistry has been demonstrated as these complexes represent isolable valence intermediates similar to those observed in copper-containing enzymes.

ASSOCIATED CONTENT

Supporting Information

The Supporting Information is available free of charge on the ACS Publications website at DOI: 10.1021/acs.inorgchem.5b01161. X-ray crystallographic data for complexes **2**−**4** have been deposited at the Cambridge Crystallographic Data Centre.

X-ray crystallographic data including structures. (CIF)
EPR as well as UV−vis−NIR and Raman spectroscopic data. DFT-calculated spin-Hamiltonian parameters and absorption spectra. (PDF)

AUTHOR INFORMATION

Corresponding Authors

*E-mail: walenskyj@missouri.edu. (J.R.W.)
*E-mail: wantholi@mcw.edu. (W.E.A.)
*E-mail: adam.fiedler@marquette.edu. (A.T.F.)

Notes

The authors declare no competing financial interest.

ACKNOWLEDGMENTS

We gratefully acknowledge the Univ. of Missouri College of Arts & Sciences Alumni Faculty Incentive Grant as well as the Nuclear Forensics Education Award Program for startup funds (J.R.W.). A.T.F. thanks the National Science Foundation (CHE-1056845) for financial support. The EPR facilities are supported by the National Biomedical EPR Center Grant No. EB001980 from NIH. A.C.L. was supported by a Howard Hughes Fellowship at the Univ. of Missouri, Columbia. We thank C. Reber, Univ. of Montreal, for obtaining the Raman spectrum of **2**.

REFERENCES

(1) Rosenzweig, A. C.; Sazinsky, M. H. *Curr. Opin. Struct. Biol.* **2006**, *16*, 729.
(2) Kroneck, P. M.; Antholine, W. A.; Riester, J.; Zumft, W. G. *FEBS Lett.* **1988**, *242*, 70.

DOI: 10.1021/acs.inorgchem.5b01161
Inorg. Chem. 2015, 54, 8509−8517

(3) Cambillau, C.; Tegoni, M.; Prudencio, M.; Pereira, A. S.; Besson, S.; Moura, J. J.; Moura, I.; Brown, K. *Nat. Struct. Biol.* **2000**, *7*, 191.
(4) Hwang, H. J.; Lu, Y. *Proc. Natl. Acad. Sci. U. S. A.* **2004**, *101*, 12842.
(5) Gamelin, D. R.; Randall, D. W.; Hay, M. T.; Houser, R. P.; Mulder, T. C.; Canters, G. W.; de Vries, S.; Tolman, W. B.; Lu, Y.; Solomon, E. I. *J. Am. Chem. Soc.* **1998**, *120*, 5246.
(6) Westmoreland, T. D.; Wilcox, D. E.; Baldwin, M. J.; Mims, W. B.; Solomon, E. I. *J. Am. Chem. Soc.* **1989**, *111*, 6106.
(7) Harding, C.; McKee, V.; Nelson, J. *J. Am. Chem. Soc.* **1991**, *113*, 9684.
(8) Barr, M. E.; Smith, P. H.; Antholine, W. E.; Spencer, B. *J. Chem. Soc., Chem. Commun.* **1993**, 1649.
(9) Harding, C.; Nelson, J.; Symons, M. C. R.; Wyatt, J. *J. Chem. Soc., Chem. Commun.* **1994**, 2499.
(10) Houser, R. P.; Young, V. G.; Tolman, W. B. *J. Am. Chem. Soc.* **1996**, *118*, 2101.
(11) Breeze, S. R.; Wang, S. *Inorg. Chem.* **1996**, *35*, 3404.
(12) Setsune, J.-I.; Yokoyama, T.; Muraoka, S.; Huang, H.-W.; Sakurai, T. *Angew. Chem., Int. Ed.* **2000**, *39*, 1115.
(13) Zhang, X.-M.; Tong, M.-L.; Chen, X.-M. *Angew. Chem., Int. Ed.* **2002**, *41*, 1029.
(14) Dong, G.; Chun-qi, Q.; Chun-ying, D.; Ke-liang, P.; Qing-jin, M. *Inorg. Chem.* **2003**, *42*, 2024.
(15) Mukherjee, A.; Nethaji, M.; Chakravarty, A. R. *Angew. Chem., Int. Ed.* **2004**, *43*, 87.
(16) Zhan, S.-Z.; Li, W.; Wang, B.-M.; Zhang, R.-L.; Kunag, W.-F. *J. Coord. Chem.* **2007**, *60*, 2747.
(17) Solomon, E. I.; Xie, X.; Dey, A. *Chem. Soc. Rev.* **2008**, *37*, 623.
(18) Mooibroek, T. J.; Aromí, G.; Quesada, M.; Roubeau, O.; Gamez, P.; DeBeer George, S.; van Slageren, J.; Yasin, S.; Ruiz, E.; Reedijk, J. *Inorg. Chem.* **2009**, *48*, 10643.
(19) Torelli, S.; Orio, M.; Pécaut, J.; Jamet, H.; Le Pape, L.; Ménage, S. *Angew. Chem., Int. Ed.* **2010**, *49*, 8249.
(20) Bakhoda, A.; Safari, N.; Amani, V.; Khavasi, H. R.; Gheidi, M. *Polyhedron* **2011**, *30*, 2950.
(21) Kirillov, A. M.; Filipowicz, M.; Guedes da Silva, M. F. C.; Kłak, J.; Smoleński, P.; Pombeiro, A. J. L. *Organometallics* **2012**, *31*, 7921.
(22) Majouga, A. G.; Beloglazkina, E. K.; Moiseeva, A. A.; Shilova, O. V.; Manzheliy, E. A.; Lebedeva, M. A.; Davies, E. S.; Khlobystov, A. N.; Zyk, N. V. *Dalton Trans.* **2013**, *42*, 6290.
(23) Gagne, R. R.; Koval, C. A.; Smith, T. J.; Cimolino, M. C. *J. Am. Chem. Soc.* **1979**, *101*, 4571.
(24) Gagne, R. R.; Henling, L. M.; Kistenmacher, T. J. *Inorg. Chem.* **1980**, *19*, 1226.
(25) Karlin, K. D.; Gan, Q.-f.; Tyeklar, Z. *Chem. Commun.* **1999**, 2295.
(26) LeCloux, D. D.; Davydov, R.; Lippard, S. J. *Inorg. Chem.* **1998**, *37*, 6814.
(27) He, C.; Lippard, S. J. *Inorg. Chem.* **2000**, *39*, 5225.
(28) Gupta, R.; Zhang, Z. H.; Powell, D.; Hendrich, M. P.; Borovik, A. S. *Inorg. Chem.* **2002**, *41*, 5100.
(29) Hagadorn, J. R.; Zahn, T. I.; Que, L., Jr.; Tolman, W. B. *Dalton Trans.* **2003**, 1790.
(30) Jiang, X.; Bollinger, J. C.; Baik, M.-H.; Lee, D. *Chem. Commun.* **2005**, 1043.
(31) Mankad, N. P.; Antholine, W. E.; Szilagyi, R. K.; Peters, J. C. *J. Am. Chem. Soc.* **2009**, *131*, 3878.
(32) Yang, L.; Powell, D. R.; Klein, E. L.; Grohmann, A.; Houser, R. P. *Inorg. Chem.* **2007**, *46*, 6831.
(33) Lo, S. M. F.; Chui, S. S. Y.; Shek, L.-Y.; Lin, Z.; Zhang, X. X.; Wen, G.-h.; Williams, I. D. *J. Am. Chem. Soc.* **2000**, *122*, 6293.
(34) Zhu, Y.; Wang, W.-y.; Guo, M.-w.; Li, G.; Lu, H.-j. *Inorg. Chem. Commun.* **2011**, *14*, 1432.
(35) Kim, K. H.; Ueta, T.; Okubo, T.; Hayami, S.; Anma, H.; Kato, K.; Shimizu, T.; Fujimori, J.; Maekawa, M.; Kuroda-Sowa, T. *Chem. Lett.* **2011**, *40*, 1184.
(36) van Albada, G. A.; Mutikainen, I.; Ghazzali, M.; Al-Farhan, K.; Reedijk, J. *Dalton Trans.* **2012**, *41*, 4566.
(37) Lewis, E. A.; Tolman, W. B. *Chem. Rev.* **2004**, *104*, 1047.
(38) Cramer, C. J.; Tolman, W. B. *Acc. Chem. Res.* **2007**, *40*, 601.
(39) Fukuzumi, S.; Tahsini, L.; Lee, Y.-M.; Ohkubo, K.; Nam, W.; Karlin, K. D. *J. Am. Chem. Soc.* **2012**, *134*, 7025.
(40) Cotton, F. A.; Feng, X.; Matusz, M.; Poli, R. *J. Am. Chem. Soc.* **1988**, *110*, 7077.
(41) Lim, B. S.; Rahtu, A.; Park, J.-S.; Gordon, R. G. *Inorg. Chem.* **2003**, *42*, 7951.
(42) Lane, A. C.; Vollmer, M. V.; Laber, C. H.; Melgarejo, D. Y.; Chiarella, G. M.; Fackler, J. P.; Yang, X.; Baker, G. A.; Walensky, J. R. *Inorg. Chem.* **2014**, *53*, 11357.
(43) *Apex II Suite;* Bruker AXS Ltd.: Madison, WI, 2006.
(44) Bruker-Nonius. *APEXII,* v2008 4−0 ed.; Bruker-Nonius Inc.: Madison, WI, 2008.
(45) Barbour, L. J. *J. Supramol. Chem.* **2001**, *1*, 189.
(46) Stoll, S.; Schweiger, A. *J. Magn. Reson.* **2006**, *178*, 42.
(47) Neese, F. *ORCA,* 2.9 ed.; Max Planck Institute for Chemical Energy Conversion: Muelheim, Germany, 2012.
(48) Becke, A. D. *J. Chem. Phys.* **1993**, *98*, 5648.
(49) Lee, C. T.; Yang, W. T.; Parr, R. G. *Phys. Rev. B: Condens. Matter Mater. Phys.* **1988**, *37*, 785.
(50) Schafer, A.; Horn, H.; Ahlrichs, R. *J. Chem. Phys.* **1992**, *97*, 2571.
(51) Schafer, A.; Huber, C.; Ahlrichs, R. *J. Chem. Phys.* **1994**, *100*, 5829.
(52) The "core properties" basis set is derived from the TurboMole DZ basis set developed by Ahlrichs and co-workers. It was obtained from the basis set library under ftp.chemie.unikarlsruhe.de/pub/basen.
(53) Neese, F. *J. Chem. Phys.* **2001**, *115*, 11080.
(54) Neese, F. *J. Chem. Phys.* **2003**, *118*, 3939.
(55) Neese, F. *Curr. Opin. Chem. Biol.* **2003**, *7*, 125.
(56) Sinnecker, S.; Slep, L. D.; Bill, E.; Neese, F. *Inorg. Chem.* **2005**, *44*, 2245.
(57) Laaksonen, L. *J. Mol. Graphics* **1992**, *10*, 33.
(58) Stratmann, R. E.; Scuseria, G. E.; Frisch, M. J. *J. Chem. Phys.* **1998**, *109*, 8218.
(59) Casida, M. E.; Jamorski, C.; Casida, K. C.; Salahub, D. R. *J. Chem. Phys.* **1998**, *108*, 4439.
(60) Bauernschmitt, R.; Ahlrichs, R. *Chem. Phys. Lett.* **1996**, *256*, 454.
(61) Hirata, S.; Head-Gordon, M. *Chem. Phys. Lett.* **1999**, *314*, 291.
(62) Hirata, S.; Head-Gordon, M. *Chem. Phys. Lett.* **1999**, *302*, 375.
(63) Abdou, H. E.; Mohamed, A. A.; Fackler, J. P. *Inorg. Chem.* **2007**, *46*, 9692.
(64) Gossage, R. A.; Ryabov, A. D.; Spek, A. L.; Stufkens, D. J.; van Beek, J. A. M.; van Eldik, R.; van Koten, G. *J. Am. Chem. Soc.* **1999**, *121*, 2488.
(65) Zhao, S.-B.; Wang, R.-Y.; Wang, S. *Inorg. Chem.* **2006**, *45*, 5830.
(66) Zhao, S.-B.; Wang, R.-Y.; Wang, S. *Organometallics* **2009**, *28*, 2572.
(67) Sakow, D.; Baabe, D.; Böker, B.; Burghaus, O.; Funk, M.; Kleeberg, C.; Menzel, D.; Pietzonka, C.; Bröring, M. *Chem. - Eur. J.* **2014**, *20*, 2913.
(68) Bowmaker, G. A.; Di Nicola, C.; Pettinari, C.; Skelton, B. W.; Somers, N.; White, A. H. *Dalton Trans.* **2011**, *40*, 5102.
(69) Blanchard, S.; Neese, F.; Bothe, E.; Bill, E.; Weyhermüller, T.; Wieghardt, K. *Inorg. Chem.* **2005**, *44*, 3636.
(70) Ditri, T. B.; Carpenter, A. E.; Ripatti, D. S.; Moore, C. E.; Rheingold, A. L.; Figueroa, J. S. *Inorg. Chem.* **2013**, *52*, 13216.
(71) Herrmann, W. A.; Thiel, W. R.; Herdtweck, E. *J. Organomet. Chem.* **1988**, *353*, 323.
(72) Cunningham, D.; McArdle, P.; Mitchell, M.; Ní Chonchubhair, N.; O'Gara, M.; Franceschi, F.; Floriani, C. *Inorg. Chem.* **2000**, *39*, 1639.
(73) Hay, M. T.; Ang, M. C.; Gamelin, D. R.; Solomon, E. I.; Antholine, W. E.; Ralle, M.; Blackburn, N. J.; Massey, P. D.; Wang, X.; Kwon, A. H.; Lu, Y. *Inorg. Chem.* **1998**, *37*, 191.
(74) Beinert, H.; Griffiths, D. E.; Wharton, D. C.; Sands, R. H. *J. Biol. Chem.* **1962**, *237*, 2337.

DOI: 10.1021/acs.inorgchem.5b01161
Inorg. Chem. 2015, 54, 8509−8517

(75) Robin, M. B.; Day, P. In *Advances in Inorganic Chemistry and Radiochemistry;* Emeléus, H. J., Sharpe, A. G., Eds.; Academic Press: Waltham, MA, 1968; Vol. *10*, p 247.
(76) Neese, F.; Zumft, W. G.; Antholine, W. E.; Kroneck, P. M. H. *J. Am. Chem. Soc.* **1996**, *118*, 8692.
(77) Iwata, S.; Ostermeier, C.; Ludwig, B.; Michel, H. *Nature* **1995**, *376*, 660.
(78) Cole, A. P.; Root, D. E.; Mukherjee, P.; Solomon, E. I.; Stack, T. D. P. *Science* **1996**, *273*, 1848.
(79) Biswas, A.; Saha, R.; Ghosh, A. *CrystEngComm* **2011**, *13*, 5342.
(80) Houser, R. P.; Tolman, W. B. *Inorg. Chem.* **1995**, *34*, 1632.
(81) Di Francesco, G. N.; Gaillard, A.; Ghiviriga, I.; Abboud, K. A.; Murray, L. J. *Inorg. Chem.* **2014**, *53*, 4647.

DOI: 10.1021/acs.inorgchem.5b01161
Inorg. Chem. 2015, 54, 8509−8517